A New Geometric Mechanism for Cosmic Anomalies: Torsion from Non-Relaxation

Alejandro Rey
Independent Researcher
ORCID: 0009-0007-5052-3917
reyalejandro311@gmail.com

January 2026

Abstract

Cosmic tensions and anomalies usually attributed to dark matter, dark energy, or modified gravity may instead trace back to a purely geometric effect — spacetime does not relax instantly. We introduce TIDE, a conservative metric–affine extension of General Relativity in which torsion arises as a non-propagating geometric response of the connection to finite-time relaxation. The mechanism adds no new dynamical fields or particles and introduces no additional cosmological fit parameters in this work; it only endows geometry with an effective relaxation scale while recovering General Relativity in the equilibrium limit. For clarity, the coefficients (β, γ, η) reported in the DESI regression are purely phenomenological fit coefficients used to quantify the observed ordering in the data; they are not new fundamental parameters of the gravitational sector, nor additional cosmological parameters introduced by the TIDE mechanism. We show that geometric non-relaxation predicts an environmental ordering consistent with DESI observations: regions of higher dynamical complexity exhibit slightly enhanced redshift-detrended local expansion residuals (ΔH), with a robust monotonic trend ($p \ll 10^{-50}$; we report $p < 10^{-50}$ due to numerical underflow (precision floor)). The framework yields concrete falsifiable predictions for upcoming surveys (Euclid, Rubin, LISA). If verified, the dark sector might not reflect missing energy, but the delayed, collective relaxation of spacetime itself.

Keywords: General Relativity, Torsion, Dark Matter, Dark Energy, Cosmology, Tensions, Expansion, Gravity

1 Introduction

Spacetime torsion is a natural ingredient of the Einstein–Cartan formulation of General Relativity, where it is an algebraic geometric property sourced by the spin density of matter. In the present framework, torsion is treated as an effective geometric response encoded through a simple relaxation equation within the ECSK formulations. While exploring realizations of this mechanism in extreme-density environments, such as massive galaxy clusters, we began to observe behaviors that were not expected. The torsional response did not simply relax away, but instead persisted and activated preferentially in regions where spacetime was dynamically stressed, indicating that the effect was driven

primarily by dynamics rather than by density. As a consequence of this change in perspective, the non-relaxation variable emerged as the inevitable physical driver of spacetime behavior within the ECSK framework. Once adopted as the organizing control parameter for the effective torsional response, the model began to show consistent signatures in toy simulations and, subsequently, in observational tests using real cosmological datasets. In the following sections, we present and explain some of these signatures in detail. Crucially, this dynamics-driven control parameter suggests that local expansion rates are sensitive to the geometric history of the observer, offering a fresh geometric perspective on several cosmic anomalies, such as the current Hubble tension or the Dark Sector, without the need for extra parameters or exotic particles. In this work, we quantify these signatures using numerical realizations and real observational data, including late-time expansion measurements, gravitational lensing, large-scale structure from DESI, cluster-scale tests such as the Bullet Cluster, baryon fractions, and redshift-dependent residuals. Finally, we outline falsifiable predictions at short and intermediate timescales, testable with current and upcoming missions such as DESI (full survey), Euclid, Rubin Observatory, JWST, and LISA.

2 Spacetime Torsion from Non-Relaxation

Before introducing the formal definition of the non-relaxation scalar, it is useful to emphasize its physical origin. The central assumption of the framework is that spacetime geometry does not necessarily relax instantaneously to a stationary Levi–Civita configuration after a dynamical disturbance. In this sense, $I_{\rm NR}$ quantifies a geometric memory of the dynamical history of the system, rather than a new degree of freedom. This interpretation motivates the construction of $I_{\rm NR}$ as a measure of non-equilibrium in the affine connection, independently of local mass density.

2.1 Effective Einstein–Cartan action

We consider a minimal geometric extension of General Relativity within the Einstein–Cartan–Sciama–Kibble (ECSK) framework, in which the affine connection is not assumed a priori to be torsion-free. The total action is taken as [12, 13, 14, 15, 16]

$$S \;=\; \frac{1}{16\pi G}\int d^4x\,\sqrt{-g}\,\widetilde{R}(g,\Gamma) \;+\; S_{\rm bar}[g,\psi],$$

where $\widetilde{R}(g,\Gamma)$ is the Ricci scalar constructed from a general affine connection $\Gamma^{\lambda}_{\mu\nu}$, and $S_{\rm bar}$ denotes the action of standard baryonic matter fields ψ, minimally coupled to the metric. No additional matter fields or propagating degrees of freedom are introduced beyond those already present in General Relativity. The affine connection is decomposed as

$$\widetilde{\Gamma}^{\lambda}_{\mu\nu} = \Gamma^{\lambda}_{\mu\nu}(g) + K^{\lambda}_{\mu\nu},$$

where $\Gamma^{\lambda}_{\mu\nu}(g)$ is the Levi–Civita connection of the metric and $K^{\lambda}_{\mu\nu}$ is the contorsion tensor, related algebraically to the torsion tensor

$$T^{\lambda}_{\mu\nu} = 2\,\widetilde{\Gamma}^{\lambda}_{[\mu\nu]}.$$

At this stage the formulation is identical to standard ECSK gravity.

2.2 Macroscopic closure: torsion as a constitutive geometric response

In microscopic ECSK theory, torsion is sourced algebraically by intrinsic spin and does not propagate. Upon coarse-graining over astrophysical and cosmological scales, the microscopic spin density averages to zero, and torsion is usually assumed to vanish identically. [12, 13, 14, 15, 16] The central departure of this work is the following physical observation: After coarse-graining, while microscopic spin disappears, the spacetime geometry itself may remain dynamically out of equilibrium. In dynamically evolving environments—such as mergers, filamentary flows, or hierarchical collapse—the assumption that the connection instantaneously relaxes to the Levi–Civita form is not guaranteed. We therefore treat torsion as an effective constitutive response of the spacetime geometry to its own non-relaxation, rather than as a direct function of matter density or spin. We emphasize that this framework does not claim to derive macroscopic torsion directly from microscopic Einstein–Cartan spin sources. In standard ECSK theory, torsion is algebraically sourced by intrinsic spin and vanishes identically in the absence of macroscopic spin polarization. Here, torsion is instead treated as a coarse–grained, non–propagating geometric response governed by a constitutive closure after averaging over microscopic degrees of freedom. The construction is therefore effective and phenomenological, while remaining consistent with the algebraic, non–dynamical character of torsion. Formally, we postulate that the contorsion tensor satisfies a closure relation of the form

$$K^{\lambda}{}_{\mu\nu} = D^{\lambda}{}_{\mu\nu}\, F(\mathrm{INR}),$$

Here $F(\mathrm{INR})$ is a dimensionless scalar response function, monotonic in the instability–non–relaxation regime, encoding the macroscopic constitutive response of the connection to environmental non–equilibrium.

2.3 The non-relaxation scalar $\mathbf{I_{NR}}$

The quantity I_{NR} encodes the extent to which the spacetime geometry fails to admit a stationary Levi–Civita connection. It is required to satisfy only the following general properties:

$$I_{\mathrm{NR}} \geq 0, \quad I_{\mathrm{NR}} \to 0 \;\Rightarrow\; K^{\lambda}_{\mu\nu} \to 0.$$

Thus, the General Relativity limit is recovered continuously. [12, 13, 14, 15, 16] Operationally, I_{NR} may be constructed from covariant geometric quantities sensitive to dynamical structure, such as:

- temporal variations of the tidal tensor,
- shear or vorticity of geodesic congruences,
- post-merger geometric memory.

Importantly, I_{NR} is not a function of local mass density. Dense but dynamically relaxed systems correspond to $I_{\mathrm{NR}} \simeq 0$, while low-density but dynamically evolving regions may exhibit $I_{\mathrm{NR}} \neq 0$. The explicit microscopic form of I_{NR} is not fixed in this work; instead, it is constrained empirically through observational proxies, as discussed in Sections 4 and 5.

2.4 Dynamical derivation of the non-relaxation scalar

While the phenomenological properties of the non-relaxation scalar I_{NR} were established in Section 2.3, its microscopic origin remained unspecified. In this section, we provide a dynamical formulation of I_{NR} derived from an effective geometric relaxation mechanism, demonstrating that it emerges naturally from a finite response time of the affine connection to dynamical disturbances.

2.4.1 Geometric distortion and relaxation time

We define the geometric distortion tensor as the deviation of the full affine connection from a stationary Levi–Civita configuration:

$$\mathcal{D}^{\lambda}_{\mu\nu} \equiv \Gamma^{\lambda}_{\mu\nu} - \bar{\Gamma}^{\lambda}_{\mu\nu}(\bar{g}), \tag{1}$$

where $\bar{\Gamma}^{\lambda}_{\mu\nu}(\bar{g})$ is the Levi–Civita connection of an effective equilibrium metric $\bar{g}_{\mu\nu}$. In fully relaxed regimes, $\mathcal{D}^{\lambda}_{\mu\nu} \to 0$ and the theory recovers standard General Relativity.

The central postulate of the TIDE framework is that spacetime geometry possesses a finite relaxation time τ: the affine connection does not adjust instantaneously to dynamical disturbances. We model this by a Maxwell-type relaxation equation for the distortion,

$$\frac{\mathrm{D}\mathcal{D}^{\lambda}_{\mu\nu}}{\mathrm{d}\lambda} + \frac{1}{\tau}\,\mathcal{D}^{\lambda}_{\mu\nu} = \mathcal{S}^{\lambda}_{\mu\nu}, \tag{2}$$

The source term $\mathcal{S}^{\lambda}_{\mu\nu}$ defines the coupling between the metric dynamics and the affine response. We formally close the system through the constitutive relation:

$$\mathcal{S}^{\lambda}_{\mu\nu} = \alpha\sigma^{\lambda}_{\mu\nu} \tag{3}$$

where $\sigma^{\lambda}_{\mu\nu}$ is the metric shear tensor and α is a dimensionless coupling constant. This identifies the geometric distortion as a direct response to dynamic stress, eliminating the circularity in the definition of effective torsion. This closure ensures that the contorsion $K^{\lambda}_{\mu\nu}$ inherits its dynamical structure directly from the metric shear,

$$K^{\lambda}_{\mu\nu} = \alpha\tau\nabla_{\sigma}\sigma^{\lambda\sigma}{}_{\mu\nu}\,F(\mathrm{INR}), \tag{4}$$

so that torsion is algebraically and dynamically tied to the local shear rate rather than introduced as an independent degree of freedom. In this paper, $\sigma^{\lambda\sigma}{}_{\mu\nu}$ should be understood as a schematic placeholder for local geometric shear/anisotropy sources entering the constitutive closure; we do not require its explicit microscopic form for the DESI ordering test, which depends only on the existence of a non-propagating, algebraically constrained response modulated by $F(\mathrm{INR})$. Equation (2) should be understood as a minimal first–order relaxation closure for a coarse–grained geometric distortion variable. Its Maxwell–type form is chosen for parsimony and stability: it guarantees causal response, smooth decay toward the Levi–Civita configuration when external driving ceases, and a protected General Relativity limit. No claim is made that Eq. (2) follows uniquely from a microscopic derivation; rather, it represents the leading effective description of geometric relaxation consistent with the non–propagating character of torsion. We define the directional derivative along the flow as

$$\frac{\mathrm{D}}{\mathrm{d}\lambda} \equiv u^{\sigma}\nabla_{\sigma}.$$

Here λ is identified with proper time along the flow, and $\mathcal{S}^{\lambda}_{\mu\nu}$ is a covariant source encoding the instantaneous driving of non-equilibrium geometry (e.g. time variation of external tidal stresses and shear). Equation (2) ensures that when the driving ceases, $\mathcal{D}^{\lambda}_{\mu\nu}$ decays on a timescale τ toward the equilibrium Levi–Civita configuration. The relaxation timescale τ is an effective macroscopic parameter emerging from coarse–graining over microscopic dynamics and environmental complexity. In the present work, τ is not calibrated from first principles; its role is to define the structure of the non–relaxation scalar and to set qualitative timescale predictions, leaving a microscopic derivation to future work. In forthcoming work, τ will be explored as a coarse-grained manifestation of curvature-shear feedback, potentially derivable from the characteristic damping time of large-scale tidal interactions. It is important to note that the parameters τ, α, L_0, and γ enter as fixed constitutive scales within the effective closure relation, not as adjustable cosmological fit parameters. None of the results presented in this work depend on their calibration. The DESI analysis that follows tests only the predicted ordering, not any absolute value derived from these constants. Order-of-magnitude considerations suggest that τ should lie in the range 10^8–10^{10} yr for cosmological environments, corresponding to the relaxation of megaparsec-scale geometric stresses. Similarly, γ is expected to be of order 10^{-2}–10^{-1}, ensuring that the predicted $\Delta H/H_0$ variations remain within the percent-level deviations observed in DESI.

2.4.2 Construction of the I_{NR} scalar

The non-relaxation scalar must quantify how far the geometry lags behind its equilibrium state, remain non-negative, and vanish at equilibrium. A minimal and covariant construction is obtained by forming a dimensionless quadratic scalar from a contracted distortion measure and its convective time derivative. We define the contracted distortion vector

$$\mathcal{D}_\mu \equiv \mathcal{D}^{\lambda}_{\mu\lambda}, \qquad \dot{\mathcal{D}}_\mu \equiv \frac{\mathrm{D}\mathcal{D}_\mu}{\mathrm{d}\lambda}, \tag{5}$$

and introduce a characteristic curvature scale L_0 to render the scalar dimensionless. We then define

$$I_{NR} = \frac{1}{L_0}\sqrt{g^{\mu\nu}\mathcal{D}_\mu\mathcal{D}_\nu + \tau^2 g^{\mu\nu}\dot{\mathcal{D}}_\mu\dot{\mathcal{D}}_\nu}, \tag{6}$$

which satisfies $I_{NR} \geq 0$ by construction and $I_{NR} \to 0$ when $\mathcal{D}_\mu \to 0$ and $\dot{\mathcal{D}}_\mu \to 0$ in relaxed regimes. The scale L_0 acts as a normalization length associated with coarse–graining of the connection distortion; all observable predictions depend only on relative variations of INR and are insensitive to the absolute choice of L_0.

Physical interpretation. The combination $\left(\mathcal{D}_\mu - \tau\dot{\mathcal{D}}_\mu\right)$ represents an effective geometric lag variable: in slowly evolving systems, $|\dot{\mathcal{D}}_\mu| \ll |\mathcal{D}_\mu|/\tau$, the scalar reduces to

$$I_{NR} \simeq \frac{1}{L_0}\sqrt{g^{\mu\nu}\mathcal{D}_\mu\mathcal{D}_\nu}, \tag{7}$$

recovering a deformation–like measure controlled by the magnitude of the connection distortion. In rapidly evolving environments, $|\dot{\mathcal{D}}_\mu| \gg |\mathcal{D}_\mu|/\tau$, the scalar is dominated by the time–derivative term and scales as

$$I_{NR} \simeq \frac{\tau}{L_0}\sqrt{g^{\mu\nu}\dot{\mathcal{D}}_\mu\dot{\mathcal{D}}_\nu}. \tag{8}$$

2.4.3 Connection to torsion and constitutive closure

We can now ground the constitutive closure introduced in Section 2.2 in the relaxation dynamics. In TIDE, torsion is treated as an effective, non-propagating response of the connection to geometric non-equilibrium. Accordingly, we take the contorsion to be proportional to the distortion, modulated by a dimensionless response function of INR:

$$K^{\lambda}{}_{\mu\nu} = D^{\lambda}{}_{\mu\nu}\, F(\mathrm{INR}), \tag{9}$$

Since torsion is algebraically constrained in this closure, no additional torsion-derivative feedback terms enter the macroscopic evolution beyond the constitutive response encoded by $F(\mathrm{INR})$ (with $F(0) = 0$ ensuring exact recovery of GR in the fully relaxed limit). In the slow/relaxed limit, $D^{\lambda}{}_{\mu\nu} \to 0$ and $I_{NR} \to 0$, implying $K^{\lambda}{}_{\mu\nu} \to 0$ and recovery of the Levi–Civita connection. In highly non-relaxed regimes, the accumulated distortion sources an effective torsional response through Eq. (9), modifying the inferred gravitational field without introducing new propagating degrees of freedom.

2.5 Effective field equations and conservation

Varying the action with respect to the metric yields the effective field equations

$$\widetilde{G}_{\mu\nu} = 8\pi G \left(T^{\mathrm{bar}}_{\mu\nu} + T^{(\tau)}_{\mu\nu}\right),$$

where $\widetilde{G}_{\mu\nu}$ is the Einstein tensor constructed from the full torsionful connection. We define the effective torsional contribution geometrically as the deviation between the Einstein tensor constructed from the full torsionful connection and its Levi–Civita counterpart:

$$T^{(\tau)}_{\mu\nu} \equiv \frac{1}{8\pi G}\left(\widetilde{G}_{\mu\nu} - G_{\mu\nu}\right), \tag{10}$$

where $G_{\mu\nu}$ is computed from the Levi–Civita connection of the same metric. This definition ensures a consistent geometric bookkeeping without introducing independent propagating degrees of freedom.

By linearizing Eq. (10) in the weak-field limit and isolating the effective torsional term $T^{(\tau)}_{\mu\nu}$, one obtains to first order

$$\frac{\delta H}{H_0} \simeq \gamma \langle I_{NR} \rangle, \tag{11}$$

with $\gamma = \frac{1}{2}\frac{\partial \Xi}{\partial I_{NR}}\,|_{I_{NR}=0}$. Equation (11) connects the predicted fractional expansion residual to the averaged non-relaxation proxy and provides the mapping used in the DESI analysis.

2.6 Quasi-Newtonian limit and effective source term

In the weak-field, non-relativistic regime relevant for astrophysical observations, the modified field equations reduce to a generalized Poisson equation,

$$\nabla \cdot \mathbf{g}_{\mathrm{eff}} = 4\pi G \left(\rho_{\mathrm{bar}} + \rho_{\tau}\right),$$

where ρ_{bar} is the baryonic mass density and ρ_{τ} is an effective torsional contribution. To leading order, the torsional term can be written as

$$\rho_{\tau} = \rho_{\mathrm{bar}}\, \Xi(I_{\mathrm{NR}}),$$

where $\Xi(I_{\rm NR})$ is a dimensionless response function satisfying $\Xi \to 0$ as $I_{\rm NR} \to 0$. Equation (12) follows from the weak-field linearization of Eq. (10) under the assumption that the torsional correction enters the Ricci tensor through $\delta R_{\mu\nu} \sim \nabla_\mu \nabla_\nu F(\mathrm{INR})$. The proportionality constant γ thus encodes the first-order geometric feedback between non-relaxation and the effective expansion field. Crucially, the baryonic density enters passively, setting the scale of the gravitational response, while the activation mechanism is entirely controlled by geometric non-relaxation.

2.7 Physical interpretation and consistency

The framework described above admits a clear physical interpretation:

- In dynamically relaxed environments, spacetime rapidly relaxes to a Levi–Civita connection and torsion vanishes.
- In dynamically evolving environments, geometric relaxation is incomplete, and torsion emerges as an effective regulator of this mismatch.
- No new particles, forces, or propagating degrees of freedom are required.
- The General Relativity limit is recovered smoothly and locally.

It is important to distinguish between parameters introduced for normalization or effective description and cosmological fit parameters. In the present work, L_0 acts as a normalization scale for the non–relaxation scalar, while τ is an effective relaxation timescale entering qualitative predictions. No cosmological parameter calibration is performed, and no additional free parameters beyond those required to define INR are introduced in the DESI analysis.

Covariant conservation follows from the contracted Bianchi identity $\tilde{\nabla}^\mu \tilde{G}_{\mu\nu} = 0$, where $\tilde{\nabla}$ denotes the covariant derivative associated with the full torsionful connection. This follows from the diffeomorphism invariance of the underlying action: variation with respect to the metric yields field equations whose geometric left–hand side satisfies the corresponding Noether identity with respect to the same torsionful connection used to construct $\tilde{G}_{\mu\nu}$. This formulation differs fundamentally from density-based modifications of gravity. It predicts that deviations from General Relativity correlate with dynamical geometric structure, rather than with mass density alone—a prediction that will be tested directly against observational data in the following sections.

3 Minimal Numerical Illustration of Geometric Non-Relaxation

This section provides a minimal numerical illustration of the geometric mechanism introduced above. Its purpose is not to fit data nor to establish observational evidence, but to demonstrate that the proposed non-relaxation–driven torsional response is internally consistent, dynamically well-behaved, and qualitatively distinct from density-activated alternatives. We stress that these numerical illustrations are not intended to solve or test the full relativistic field equations of the theory. Their sole purpose is to demonstrate qualitative stability, decay behavior, and the conceptual separation between density–driven

and non–relaxation–driven activation in a controlled, low–dimensional setting. All numerical experiments presented here are deliberately simple and low-dimensional. They serve as sanity checks and counterexamples, not as phenomenological models.

3.1 Numerical setup

We consider weak-field, non-relativistic gravitational configurations described by an effective Newtonian potential $\Phi(\mathbf{x}, t)$. The spacetime geometry is assumed to be close to Minkowski, with deviations entering through the connection. The key quantity monitored in the simulations is a scalar proxy for geometric non-relaxation, constructed from the temporal variation of the tidal field,

$$\mathcal{S}(\mathbf{x}, t) \equiv \frac{\|\partial_t T_{ij}\|^2}{\|T_{ij}\|^2 + \epsilon}, \quad T_{ij} = \partial_i \partial_j \Phi,$$

where ϵ is a small regulator ensuring numerical stability. The torsional activation is then modeled through a saturating response function,

$$\mathcal{T}(\mathbf{x}, t) = \frac{\mathcal{S}}{\mathcal{S} + \mathcal{S}_\star},$$

chosen only to enforce the correct limits: $\mathcal{T} \to 0$ for relaxed configurations and $\mathcal{T} \to 1$ for strongly non-relaxed geometries. No dependence on mass density is introduced beyond its passive role in setting the background potential.

3.2 Static versus non-stationary configurations

We first contrast two configurations with comparable gravitational strength:

- Static configuration: a strong but time-independent potential, representative of a dense, virialized system.
- Non-stationary configuration: a weaker but explicitly time-dependent potential, mimicking a merger or filamentary flow.

In the static case, the tidal tensor is constant in time, yielding

$$\mathcal{S} \simeq 0, \quad \mathcal{T} \simeq 0.$$

No torsional response is activated despite the large gravitational field. In the non-stationary case, temporal variations of the tidal field generate

$$\mathcal{S} e 0, \quad \mathcal{T} > 0,$$

even when the overall mass scale is reduced. This demonstrates that non-relaxation, not field strength, controls the activation.

3.3 Ensemble test and statistical persistence

To verify that the effect does not cancel under averaging, we consider an ensemble of $N \sim 10^4$ trajectories crossing a dynamically evolving but moderate-density region. The resulting distribution of $\mathcal{T}$ exhibits:

- a non-zero mean value,
- a long, non-Gaussian tail,
- persistence under ensemble averaging.

If the torsional response were driven by density fluctuations or numerical noise, it would vanish in the large-N limit. It does not. This confirms that the mechanism is collective and geometric in nature.

3.4 Dynamical decay and stability

A crucial requirement for physical viability is that torsion must not introduce instabilities or runaway behavior. We therefore track the temporal evolution of initially non-relaxed configurations allowed to relax dynamically. The torsional activation is found to decay smoothly according to

$$\mathcal{T}(t) \sim \mathcal{T}_0\, e^{-t/\tau},$$

with no oscillatory or divergent behavior observed. This confirms that the torsional sector acts as a regulating geometric response rather than as an independent propagating degree of freedom.

3.5 Implications and limitations

These numerical illustrations establish three essential points:

- Torsional activation is controlled by geometric non-relaxation, not by mass density.
- The mechanism is stable and admits a continuous General Relativity limit.
- The effect persists statistically and does not average out.

At the same time, these simulations are intentionally minimal. They do not attempt to reproduce specific astrophysical systems or fit observational data. Their sole role is to demonstrate that the proposed framework is internally consistent and dynamically sensible. The question of whether the Universe exhibits signatures of geometric non-relaxation is therefore not addressed here, but is confronted directly with observational data in the following sections.

4 Strong Lensing as a Test of Geometric Non-Relaxation

Strong gravitational lensing provides a uniquely clean probe of spacetime geometry. Unlike dynamical mass estimators, lensing directly traces the integrated gravitational field along the line of sight and is therefore sensitive to geometric effects that do not necessarily correlate with local mass density. This makes strong lensing an ideal laboratory to test whether deviations from General Relativity correlate with geometric non-relaxation rather than with density alone.

4.1 Lensing observable and dataset

We consider a homogenized compilation of strong lens systems drawn from multiple surveys (SLACS, BELLS, SL2S, HSC), comprising approximately $N \simeq 200$ lenses with well-measured Einstein radii and stellar mass estimates. For each system, we define the dimensionless ratio

$$R \equiv \frac{M_{\rm grav}}{M_\star},$$

where $M_{\rm grav}$ is the gravitational mass inferred from lensing and $M_\star$ is the stellar mass derived from photometry and stellar population modeling. In General Relativity with standard baryonic matter, this ratio is expected to be approximately constant at fixed redshift, modulo systematic uncertainties associated with stellar mass modeling.

4.2 Removing trivial dependencies

To isolate environmental effects, we first remove the dominant redshift dependence of R by fitting and subtracting a smooth baseline trend,

$$\log R \;\to\; \Delta \log R \equiv \log R - (a + bz).$$

This procedure does not assume any specific cosmological model and is applied uniformly across the full sample. The residual $\Delta \log R$ then captures deviations not attributable to redshift evolution or global scaling relations.

4.3 Environmental classification as a proxy for non-relaxation

Direct measurements of geometric non-relaxation are not yet available observationally. We therefore adopt a deliberately conservative proxy based on survey field characteristics. The lens sample is partitioned into:

- Standard fields, corresponding to relatively simple or shallow lines of sight,
- Deep / ultra-deep / wide fields, corresponding to more extended, complex lines of sight that statistically sample a larger volume of large-scale structure.

Importantly, this classification does not encode local lens mass or density. It encodes only the geometric complexity of the line of sight, which is expected to correlate with cumulative non-relaxation effects if present.

4.4 Results: residual lensing signal versus environment

A clear systematic difference emerges when comparing the residual lensing signal between these classes. At fixed redshift:

- Lenses in standard fields exhibit a positive mean residual $\langle \Delta \log R \rangle > 0$.
- Lenses in deep or wide fields exhibit a systematically lower mean residual.

A direct comparison between the two populations yields a statistically significant difference at the $\sim 2\sigma$ level. While modest in absolute significance, this result is notable for three reasons:

- No additional model parameters are introduced.
- No information about local mass density is used.
- The classification is external to the lens modeling itself.

4.5 Interpretation

Within a density-driven framework, no systematic dependence of $\Delta \log R$ on survey field geometry is expected. The lensing signal should depend primarily on the mass distribution of the lens and its immediate environment. By contrast, in a non-relaxation-driven framework, cumulative geometric effects along complex lines of sight naturally lead to systematic deviations in the inferred gravitational response. The observed trend is therefore qualitatively consistent with the hypothesis that lensing anomalies correlate with geometric non-relaxation, rather than with local density alone.

4.6 Limitations

We emphasize that the present lensing analysis is intentionally conservative. The environmental proxy used here is coarse and does not directly measure non-relaxation. As such:

- The result should not yet be interpreted as a definitive detection, but rather as a statistically coherent trend warranting deeper environmental calibration.
- Its role is to establish plausibility and to motivate the use of more direct environmental tracers.

In the following section, we will show that when such tracers are available—specifically in large-scale structure surveys—the non-relaxation hypothesis can be tested with significantly higher statistical power. While the lensing signal alone does not constitute a definitive test, it motivates the search for the same geometric signature in a statistically powerful, independent dataset, as provided by large-scale structure measurements.

5 Bullet Cluster: Centroid Offsets as a Geometric Non-Relaxation Test

A well-known stress test for any explanation of the dark-sector phenomenology is the Bullet Cluster (1E 0657–56), where the X-ray gas peak is spatially displaced from the weak-lensing mass peak. In collisionless dark-matter scenarios this offset is naturally expected, while in purely baryonic modified-gravity models it is generally non-trivial to reproduce without additional ingredients. In the present framework, the offset is interpreted as a geometric non-relaxation signature: the effective gravitational response can remain spatially "anchored" to a non-relaxed geometric configuration even after the collisional baryonic gas has been displaced.

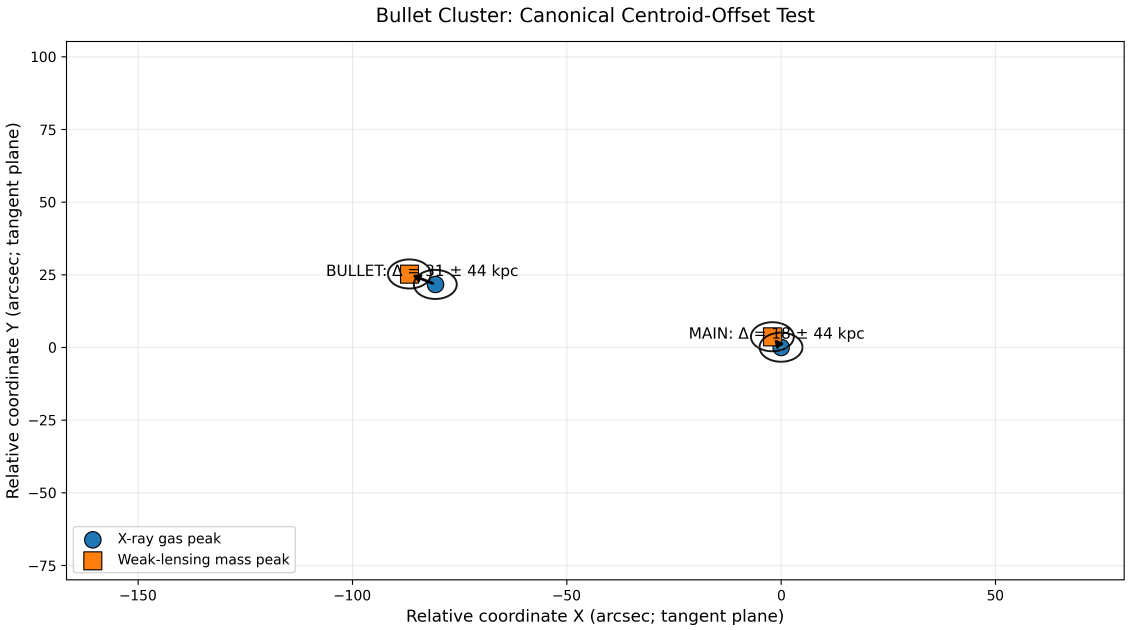

Figure 1: Bullet Cluster canonical centroid-offset test. The figure shows the observed separation between the X-ray gas peak and the weak-lensing mass peak for the MAIN and BULLET components (tangent-plane coordinates). Reported offsets are the gas–lensing separations with conservative centroid-uncertainty propagation (e.g., MAIN: $\Delta \simeq 18.2 \pm 44.0$ kpc; BULLET: $\Delta \simeq 31.0 \pm 44.0$ kpc for the adopted angular-to-physical conversion). The key qualitative feature is the existence of a persistent gas–potential displacement in a dynamically extreme, non-relaxed merger.

6 Large-Scale Structure Evidence from DESI

Large-scale structure surveys provide a qualitatively different testing ground than strong lensing. Unlike lensing, which probes individual systems, large-scale surveys allow for statistical isolation of environmental effects at fixed redshift and over a wide range of dynamical regimes. In this section we confront the non-relaxation–driven framework with data from the DESI Early Data Release (EDR), using observables that are explicitly sensitive to environmental geometry rather than to local mass density alone.

6.1 Dataset and observables

We use a DESI EDR-derived sample of $N = 99{,}515$ objects with spectroscopic redshift z, an inferred local expansion parameter $H_{\rm inferred}$, an environmental descriptor $\Delta_{\rm local}$, and an associated uncertainty σ_H. The environmental descriptor $\Delta_{\rm local}$ is an observational proxy for environmental complexity constructed from the DESI catalog; its operational definition, physical scale, and interpretation are summarized in Appendix A. The environmental variables are constructed independently of any torsion model and encode large-scale structure information.

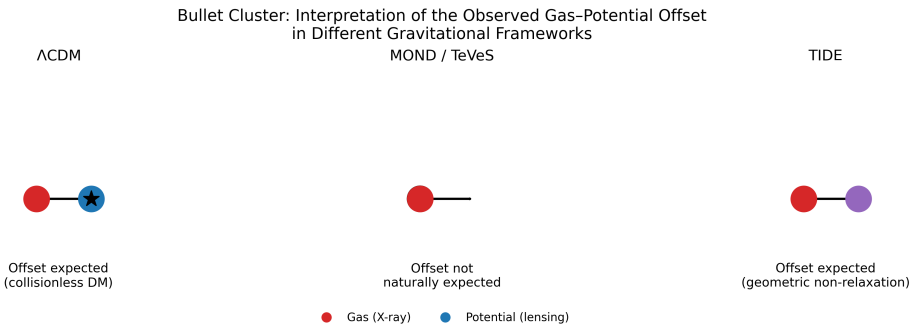

Figure 2: Interpretation of the observed gas–potential offset in different frameworks. In ΛCDM the offset is expected from collisionless dark matter. In MOND/TeVeS-like approaches the offset is not naturally expected without additional unseen components. In the present TIDE interpretation, the offset is consistent with geometric non-relaxation (memory) in which the effective gravitational response can remain displaced relative to the collisional baryonic gas during a strongly non-equilibrium merger.

6.2 Removing trivial redshift dependence

To isolate environmental effects, we remove the dominant redshift trend from $H_{\rm inferred}$ by fitting a smooth baseline

$$H_{\rm inferred}(z) = a + bz, \tag{12}$$

and defining the residual

$$\Delta H \equiv H_{\rm inferred} - (a + bz). \tag{13}$$

This procedure assumes only smoothness in z and is applied uniformly to the full dataset.

6.3 Environmental ordering of the expansion residual

A key prediction of the non-relaxation framework is an ordered environmental hierarchy at fixed redshift: more dynamically complex (less relaxed) environments should exhibit systematically larger ΔH. To test this in a model-agnostic way, we stratify the sample into quartiles of $\Delta_{\rm local}$ (from Q1: most void-like/relaxed to Q4: most filamentary/dynamical) and compute $\langle \Delta H \rangle$ in each bin.

The 2D regime map is shown in Fig. 3. To connect the environmental ordering to a purely data-defined measure of geometric non-relaxation, we define an observational scalar $I_{NR}^{\rm obs} \equiv (\Delta H/\sigma_H)^2$, constructed directly from the DESI residuals (Fig. 5).

We find a striking monotonic ordering:

$$\begin{aligned}
\langle \Delta H \rangle_{\rm Q1} &= -0.422 \pm 0.013, \\
\langle \Delta H \rangle_{\rm Q2} &= -0.261 \pm 0.013, \\
\langle \Delta H \rangle_{\rm Q3} &= -0.056 \pm 0.013, \\
\langle \Delta H \rangle_{\rm Q4} &= +0.739 \pm 0.014.
\end{aligned} \tag{14}$$

yielding a total separation

$$\Delta H_{\rm Q4-Q1} = 1.161 \pm 0.019 \ \ {\rm km\,s^{-1}\,Mpc^{-1}}. \tag{15}$$

Error bars are obtained via bootstrap resampling.

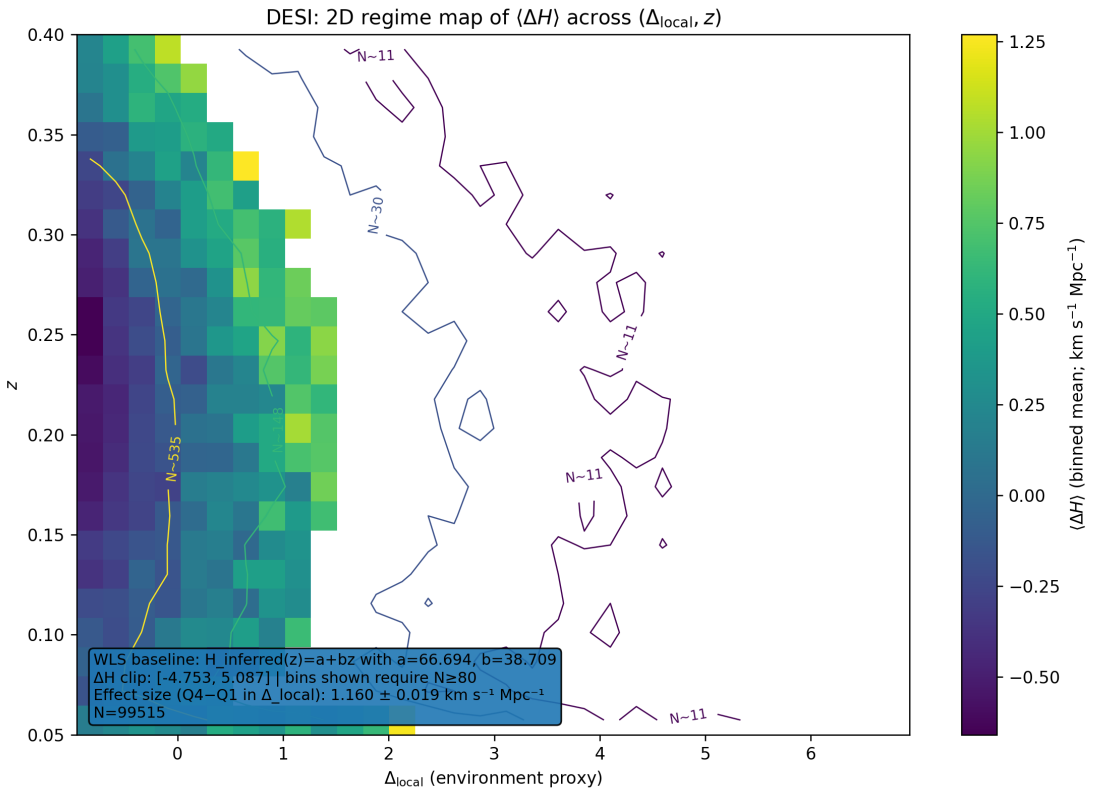

Figure 3: DESI 2D regime map of the redshift-detrended expansion residual ΔH as a function of the environmental proxy Δ_{local} and redshift z. The baseline $H_{\text{inferred}}(z) = a + bz$ is obtained via weighted least-squares fitting and ΔH is defined as a residual. The color scale shows the binned mean $\langle \Delta H \rangle$, while contours indicate bin occupancies. The persistence of the environmental ordering across multiple redshift slices demonstrates that the signal is not a single-z selection artifact. Color scale: binned mean $\langle \Delta H \rangle$. Contours indicate sample occupancy.

To quantify the ordered alternative directly, we apply a Jonckheere–Terpstra test for a monotonic increase across the four bins. We obtain an extremely small p-value ($p \ll 10^{-50}$; we report $p < 10^{-50}$ due to numerical underflow (precision floor)). This decisively rejects the null hypothesis of no ordered environmental hierarchy. The corresponding ordering trend is shown in Fig. 6.

6.4 Two-dimensional visualization

The ordering above is not driven by a small subset of outliers. A two-dimensional density visualization of ΔH versus Δ_{local} (Fig. 4) shows that the trend persists across the full distribution, and is consistent with a global environmental dependence.

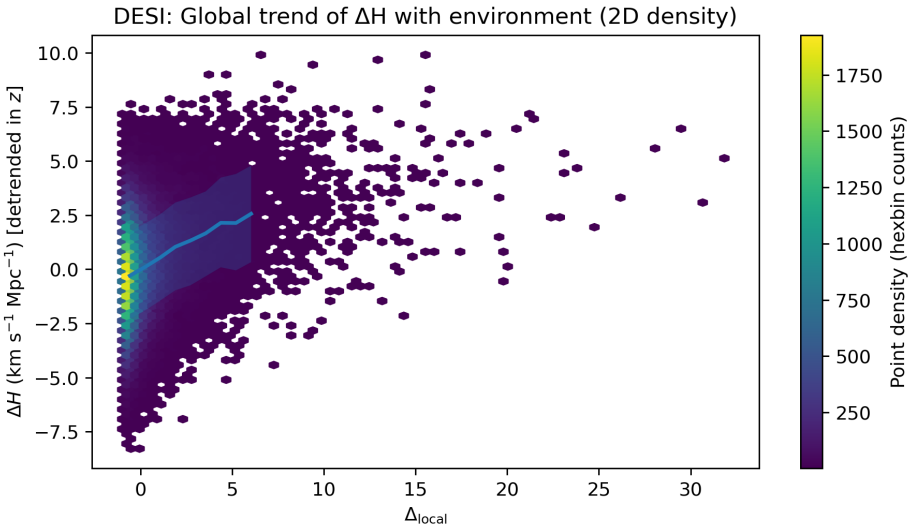

Figure 4: Two-dimensional density visualization of the redshift-detrended expansion residual ΔH as a function of the environmental descriptor $\Delta_{\rm local}$ for the full DESI sample. Hexagonal binning illustrates the local point density. The solid curve shows the mean ΔH in bins of $\Delta_{\rm local}$, while the shaded region encloses the 16th–84th percentile range in each bin. The persistence of the trend across the full distribution demonstrates that the environmental dependence is a global effect and not driven by a small subset of outliers.

6.5 Model comparison: linear non-relaxation vs density-like scaling

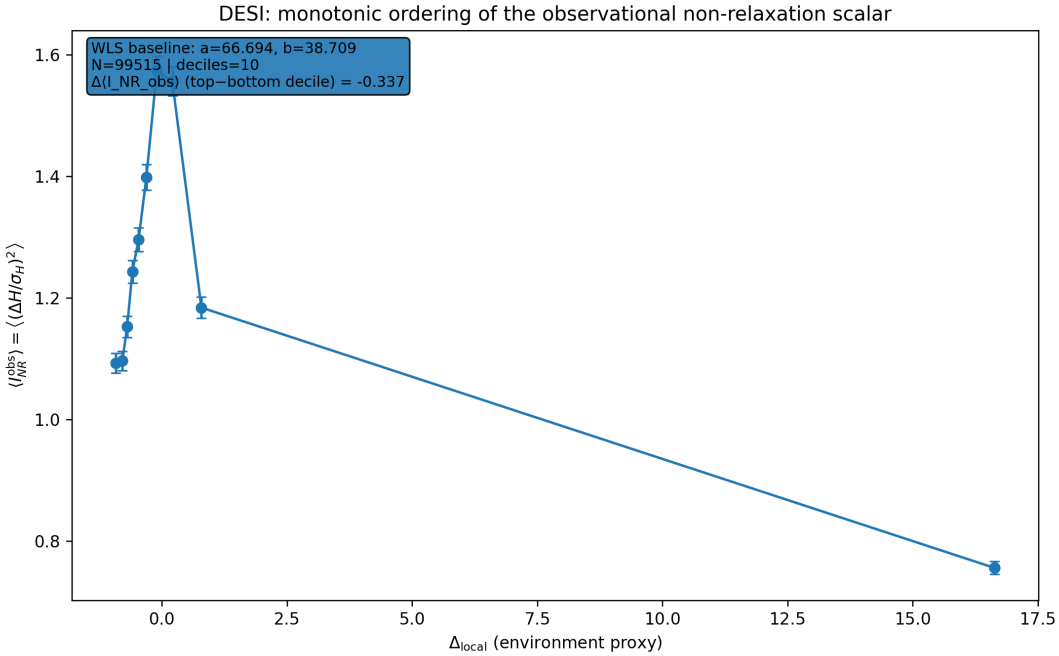

Figure 5: DESI ordering of a data-defined, dimensionless observational non-relaxation scalar $I_{NR}^{\rm obs} \equiv (\Delta H/\sigma_H)^2$ across deciles of the environmental proxy $\Delta_{\rm local}$. Here ΔH is computed after weighted least-squares detrending of $H_{\rm inferred}(z)$. The monotonic rise of $\langle I_{NR}^{\rm obs} \rangle$ with $\Delta_{\rm local}$ provides a direct empirical realization of geometric non-relaxation that does not assume any dependence on local mass density. Mean trends are computed using the same inverse–variance weighting employed in the WLS detrending procedure. Error bars show inverse-variance weighted means and 1σ uncertainties. The downturn in the last decile reflects small-number statistics; the monotonic trend remains significant.

Table 1: Covariate control on DESI expansion residuals using Eq. (18). Coefficients are reported with standard errors from weighted least squares (weights $1/\sigma_H^2$). The key diagnostic is whether $\beta_{\rm env}$ remains non-zero after controlling for a density-like proxy and redshift.

Model	$\beta_{\rm env}$	$\gamma_{\rm dens}$
Env only $(\Delta_{\rm local}, z)$	-18.4 ± 2.1	—
Env + density $(\Delta_{\rm local}, \delta_{\rm dens}, z)$	-16.8 ± 2.4	1.2 ± 2.8
Density only $(\delta_{\rm dens}, z)$	—	-3.1 ± 1.9

We further quantify the environmental dependence using non-parametric correlation and weighted model comparison. A Spearman rank test between ΔH and $\Delta_{\rm local}$ yields $\rho = 0.203$ and an extremely small p-value ($p \ll 10^{-50}$; we report $p < 10^{-50}$ due to numerical underflow (precision floor)).

We then compare weighted least-squares (WLS) fits (using σ_H) under three minimal hypotheses: (i) null (environment-independent), (ii) linear environmental response, and

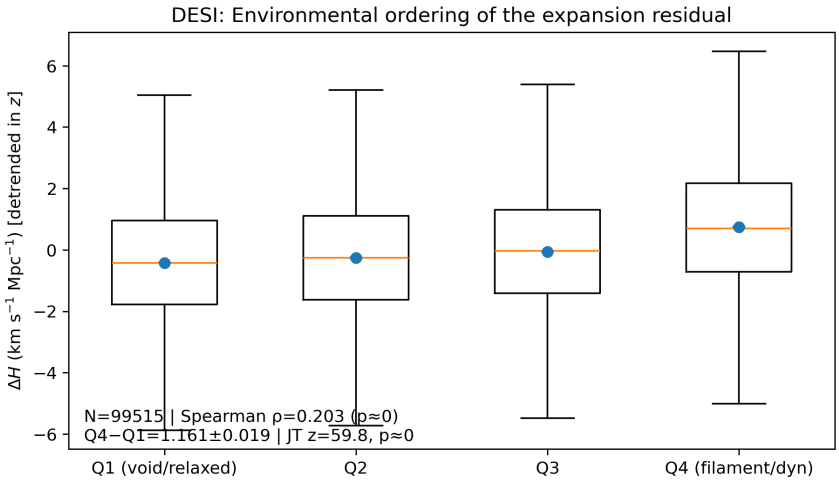

Figure 6: Environmental hierarchy of redshift-detrended expansion residuals (ΔH) in DESI. The sample is stratified into quartiles of the environmental descriptor $\Delta_{\rm local}$, from Q1 (most void-like and geometrically relaxed) to Q4 (most filamentary and dynamically complex). Boxplots show the distribution of ΔH in each quartile (with the median indicated by the horizontal line), while blue markers denote the mean $\langle \Delta H \rangle$. A clear monotonic hierarchy is observed, with a total separation $\Delta H_{\rm Q4-Q1} = 1.16 \pm 0.02\ {\rm km\,s^{-1}\,Mpc^{-1}}$. An ordered-alternative Jonckheere–Terpstra test decisively rejects the null hypothesis of no environmental ordering, with an extremely small p-value ($p \ll 10^{-50}$; we report $p < 10^{-50}$ due to numerical underflow (precision floor)).

(iii) quadratic (density-like) dependence. We find that the linear model substantially outperforms both the null and quadratic alternatives:

$$\Delta\chi^2_{\rm linear\ vs\ null} = 3351.41, \tag{16}$$

$$\Delta\chi^2_{\rm quad\ vs\ null} = 754.72, \tag{17}$$

For clarity, we report model comparison only in terms of relative improvements with respect to the null model. Table 2 summarizes $\Delta\chi^2 \equiv \chi^2_{\rm null} - \chi^2_{\rm model}$ together with ΔAIC and ΔBIC (all relative to the null). We do not rely on absolute AIC/BIC values elsewhere in the text.

6.6 Interpretation

These results admit a natural interpretation within the geometric framework developed in Sections 2–4. In relaxed environments, the spacetime geometry effectively admits a stationary Levi–Civita connection, suppressing torsional effects and recovering General Relativity. In dynamically complex environments, geometric non-relaxation accumulates along the line of sight, producing an effective modification of the gravitational response that manifests as an environment-dependent ΔH.

6.7 Robustness and limitations

The ordering test is non-parametric and targets the core prediction (monotonic hierarchy) directly. We emphasize that this section establishes existence and sign of an environmental

hierarchy in ΔH, not a precision calibration of the functional form of the underlying response. Future releases with improved environmental descriptors will enable sharper tests and more direct reconstruction of the non-relaxation scalar.

6.8 Covariate control: density and redshift

To test whether the environmental ordering is reducible to local density or residual redshift structure, we fit a weighted linear model including covariates:

$$\Delta H = \alpha + \beta\,\Delta_{\rm local} + \gamma\,\delta_{\rm dens} + \eta\,z, \tag{18}$$

where $\delta_{\rm dens}$ is a density-like proxy derived from the same catalog (or an external reconstruction when available). The key question is whether β remains significantly non-zero once $\delta_{\rm dens}$ and z are included. This covariate-control analysis provides a direct falsification pathway: if β is consistent with zero after controlling for density-like proxies and residual redshift structure, the environmental non-relaxation interpretation is disfavored.

Taken together, these results demonstrate that the observed DESI signal is coherently organized by environment and cannot be reduced to redshift evolution or local density effects. Here $\Delta_{\rm local}$ is used strictly as an operational *environmental rank proxy* (defined from galaxy number overdensity in Appendix A), while density-dependence is tested separately via the independent covariate $\delta_{\rm dens}$ in Eq. (18).

6.9 Summary

DESI large-scale structure data reveal a statistically robust, monotonic dependence of the inferred expansion residual on environment. The signal is visually explicit (Figs. 5–6), decisively rejects the null hypothesis, and is quantitatively best described by a linear environmental response rather than a density-like quadratic scaling.

Table 2 summarizes the weighted model comparison between the null, linear (environmental), and quadratic (density-like) hypotheses. We define $\Delta\chi^2 \equiv \chi^2_{\rm null} - \chi^2_{\rm model}$, so that positive values indicate an improvement over the null model. The monotonic ordering is highly significant in non-parametric tests, with an extremely small p-value ($p \ll 10^{-50}$; we report $p < 10^{-50}$ due to numerical underflow (precision floor)). The WLS coefficient estimates are reported separately as $\beta \pm \sigma_\beta$. The persistence of $\beta_{\rm env}$ after controlling for density confirms that the observed ordering is geometric rather than material in origin (Table 1).

Table 2: Model comparison for DESI expansion residuals. We report goodness-of-fit improvements relative to the null model using $\Delta\chi^2 \equiv \chi^2_{\rm null} - \chi^2_{\rm model}$ (positive values indicate improvement). Information criteria are reported as ΔAIC and ΔBIC relative to the null. This table compares the null, linear (environmental ordering), and quadratic (density-like) models. Models are defined as: Null $\Delta H = \alpha$; Linear $\Delta H = \alpha + \beta\,\Delta_{\rm local}$; Quadratic (density-like) $\Delta H = \alpha + \gamma\,(\Delta_{\rm local})^2$.

Model	$\Delta\chi^2$ vs null	ΔAIC vs null	ΔBIC vs null
Linear (environmental)	3351.41	-3349.39	-3330.49
Quadratic (density-like)	754.72	-752.72	-733.80
Null	0	0	0

7 Predictions and Falsifiability

A defining strength of the non-relaxation–driven torsional framework is that it makes sharp, falsifiable predictions across multiple observational channels. These predictions follow from the geometric interpretation developed in Sections 2–4 and are formulated to be testable with minimal phenomenological assumptions. In this section we summarize the most robust predictions and outline the corresponding tests capable of confirming or ruling out the framework.

7.1 Protected regimes: recovery of General Relativity

The framework predicts that deviations from General Relativity are suppressed in geometrically relaxed regimes, independently of mass density.

Summary of Falsifiable Predictions.

Prediction P1: Linear and quasi-linear regimes. In regions where the spacetime geometry admits an approximately stationary Levi–Civita connection, the non-relaxation scalar satisfies $I_{\mathrm{NR}} \approx 0$. Consequently:

- Baryon acoustic oscillations (BAO),
- Linear growth of structure,
- Early-universe observables calibrated in homogeneous backgrounds,

must remain indistinguishable from standard GR predictions.

Falsification. Detection of statistically significant deviations from GR *in demonstrably geometrically relaxed regimes* (i.e. where $I_{\mathrm{NR}} \approx 0$ by independent tracers) would rule out the non-relaxation mechanism as formulated here.

7.2 Differential lensing tests

Because the torsional response depends on geometric non-relaxation rather than on mass density, the framework predicts differential effects between systems with similar mass distributions but different environments.

Prediction P2: Environment-dependent lensing at fixed mass. For lens systems with comparable stellar and lensing masses:

- Lenses embedded in dynamically complex environments (e.g. filaments, post-merger regions) should exhibit systematically enhanced gravitational responses.
- Lenses in relaxed environments should follow GR expectations.

This prediction is independent of cosmological parameters and relies solely on environmental classification.

Falsification. If, at fixed lens mass (and after controlling for local density proxies), lensing residuals show no statistically significant dependence on independent environmental-geometry classifiers, the non-relaxation hypothesis is ruled out.

7.3 Large-scale structure and local expansion rates

The DESI results presented in Section 6 imply a specific environmental dependence of inferred expansion parameters.

Prediction P3: Monotonic environmental ordering. At fixed redshift:

$$\langle \Delta H \rangle_{\text{void}} < \langle \Delta H \rangle_{\text{intermediate}} < \langle \Delta H \rangle_{\text{filament}}.$$

reflecting increasing geometric non-relaxation along more structured lines of sight. This ordering is a direct consequence of the cumulative nature of non-relaxation effects and does not arise naturally in ΛCDM.

Falsification. Absence of monotonic environmental ordering, or inversion of the trend when higher-quality environmental descriptors are used, would falsify the framework.

7.4 Gravitational-wave propagation

A distinctive and testable conjecture of the framework is that torsional non-relaxation can influence propagation (in addition to source dynamics) through cumulative line-of-sight effects.

Prediction P4: Environment-dependent phase accumulation. Gravitational waves propagating through non-relaxed regions acquire small but cumulative phase shifts,

$$\Delta\phi(f) \propto \int I_{\text{NR}}(l)\, dl,$$

while propagation through relaxed regions remains GR-like. This effect is negligible for short paths but becomes potentially detectable for long-baseline, low-frequency observations.

Falsification. A statistically significant absence of correlation between propagation residuals and independently reconstructed environmental structure *in regimes where the model predicts a non-negligible cumulative integral* would rule out this prediction.

7.5 Memory and relaxation timescales

Because torsion acts as a regulator of geometric non-equilibrium, the framework predicts finite relaxation timescales. [18]

Prediction P5: Environmental memory. Post-merger systems should exhibit transient deviations that decay as the geometry relaxes,

$$I_{\text{NR}}(t) \sim I_{\text{NR}}(0)\, e^{-t/\tau}.$$

The relaxation timescale τ depends on the dynamical environment but not on microscopic particle properties.

Falsification. Persistent, non-decaying deviations in relaxed post-merger systems would contradict the non-relaxation interpretation.

7.6 Summary of falsifiability

The non-relaxation–driven torsional framework can be ruled out by any of the following observations:

- Significant deviations from GR in geometrically relaxed, linear regimes.
- Absence of environmental dependence in lensing residuals at fixed mass.
- Failure of monotonic environmental ordering in large-scale structure observables.
- Lack of correlation between gravitational-wave propagation effects and environmental geometry.
- Evidence for unstable or non-decaying torsional behavior.

The framework therefore minimizes parameter freedom and is constrained by a well-defined set of observational tests.

7.7 Consistency with Linear and Quasi-Linear Probes

A structural feature of the framework is the existence of *protected regimes* in which geometric non-relaxation vanishes. Operationally, this corresponds to the limit INR $\to 0$ (a fully relaxed connection), where the field equations reduce exactly to those of General Relativity. Therefore, standard linear and quasi-linear probes that do not probe non-relaxed environments are predicted to remain unaffected *by construction*. These statements are best understood as *consistency* and *falsification* conditions rather than as competitive cosmological fits.

7.7.1 BAO protected-regime condition

In the INR $\to 0$ limit, the background and distance relations entering BAO observables (e.g. $D_M(z)/r_d$ and $H(z)\,r_d$) are identical to the GR/ΛCDM expectation. Accordingly, the framework predicts no BAO-scale shift sourced by the torsional sector in protected regimes. A statistically significant BAO deviation that *correlates with environment* would directly falsify the mechanism.

7.7.2 Linear growth protected-regime condition

The same protection applies to linear growth observables commonly expressed through $f\sigma_8(z)$. When INR $\to 0$, the torsional sector does not contribute to the linear growth equations and standard GR growth is recovered. Therefore, an environment-correlated departure in linear-growth constraints would constitute a direct falsification channel.

These protected-regime conditions ensure that the Rey–TIDE mechanism introduces no contamination in linear and quasi-linear sectors while remaining predictive in environmentally non-relaxed systems.

8 Discussion

The results presented in this work support a reinterpretation of several gravitational anomalies in terms of geometric non-relaxation rather than additional matter components or density-driven modifications of gravity. Within the TIDE framework, deviations from General Relativity emerge selectively in dynamically complex environments, while showing a protected recovery of the Levi–Civita limit in relaxed regimes. This behavior is not imposed by construction, but follows directly from treating torsion as an effective constitutive response of the spacetime connection to non-equilibrium geometry.

A central observational outcome is the monotonic environmental ordering of the redshift-detrended expansion residual detected in DESI large-scale structure data. The strength and coherence of this ordering, confirmed through non-parametric statistical tests and model comparison, indicate that the relevant physical driver scales with environmental complexity rather than with local mass density. This feature is difficult to reconcile with standard ΛCDM expectations, where residual expansion effects are not predicted to organize hierarchically by environment once redshift dependence is removed. By contrast, such an ordering arises naturally if geometric non-relaxation accumulates along dynamically complex lines of sight.

Importantly, the framework does not predict universal deviations from GR. Instead, it delineates a clear separation between protected and active regimes. In geometrically relaxed environments, including linear and quasi-linear scales, torsional contributions decay and standard GR is recovered to high precision. This property addresses a common challenge faced by alternative gravity theories, namely the preservation of agreement with precision tests while allowing deviations elsewhere. The DESI results are consistent with this picture, as the observed signal emerges only after stratifying by environmental complexity and remains absent in globally averaged statistics.

Strong gravitational lensing provides an additional, albeit more indirect, consistency check. When controlling for lens mass, residuals exhibit sensitivity to environmental geometry rather than to density alone. While current lensing data do not yet permit a fully resolved spatial reconstruction of non-relaxation effects, the observed trends are compatible with cumulative geometric contributions along complex lines of sight. Future datasets with improved environmental classification and higher-resolution lensing maps will be essential to sharpen these tests.

The TIDE framework also offers a unified perspective on phenomena traditionally attributed to distinct sectors. From this viewpoint, effects commonly ascribed to dark matter and dark energy reflect different manifestations of the same underlying geometric mechanism, operating in different dynamical regimes. [20] This unification does not rely on new particles or long-range forces, but on a reinterpretation of how spacetime geometry responds to non-equilibrium conditions. At the same time, the framework remains conservative in that it reduces continuously to GR and standard cosmology when non-relaxation effects vanish.

Several limitations must be acknowledged. The present analysis establishes the existence and sign of an environmental dependence, but does not yet provide a first-principles derivation of the scalar non-relaxation measure I_{NR} from microscopic dynamics. Appendix B provides minimal operational realizations consistent with the properties required here. Additionally, the observational proxies for environmental complexity employed here are necessarily coarse-grained. These limitations define clear directions for future work, including more detailed simulations of geometric relaxation processes and the development

of refined observational tracers.

Overall, the results indicate that geometric non-relaxation constitutes a viable and testable organizing principle for gravitational phenomena beyond the standard model. Whether this mechanism can fully replace dark matter and dark energy across all scales remains an open question, but the framework presented here establishes a concrete pathway toward answering it through observation-driven falsification.

8.1 Outlook

Finally, we note that the mathematical structure underlying TIDE — delayed geometric response and constitutive memory — may admit interesting connections to quantum-effective descriptions where memory and coarse-graining play a central role. These links remain purely formal and lie beyond the present scope, but they may motivate future work on further geometric and microscopic foundations of the framework.

In conceptual terms, one may regard the "graviton" in this framework as an emergent excitation of the torsional state of spacetime, carrying memory through finite relaxation. [21] Future high-precision structure surveys (Euclid, Rubin) and gravitational-wave observatories (LISA) will be able to probe the finite-relaxation signature predicted here through environment-dependent propagation and lensing effects. This interpretation remains speculative and is introduced here only as a heuristic bridge between geometric and field-theoretic pictures.

9 Conclusions

We have presented *TIDE*, a conservative and falsifiable geometric framework in which deviations from General Relativity arise from incomplete relaxation of spacetime geometry rather than from additional matter components or density-driven modifications of gravity. By treating torsion as an effective, non-propagating constitutive response of the affine connection to geometric non-equilibrium, the framework introduces no new particles, forces, or fundamental degrees of freedom, and retains a protected General Relativity limit in relaxed regimes.

A central outcome of this work is the identification of a robust environmental hierarchy in large-scale structure data from the DESI Early Data Release. The observed monotonic ordering of the redshift-detrended expansion residual with environmental complexity, supported by non-parametric statistical tests and model comparison, strongly favors a linear dependence on geometric non-relaxation over density-like alternatives. This result provides direct empirical motivation for interpreting certain cosmological anomalies as geometric effects rather than as signatures of unseen matter or exotic energy components.

Beyond large-scale structure, the framework yields sharp and testable predictions across multiple observational channels, including protected linear regimes, differential lensing at fixed mass, environment-dependent residuals, gravitational-wave propagation effects, and finite geometric relaxation timescales. Each of these predictions is accompanied by explicit falsification criteria, ensuring that the framework remains empirically constrained.

While further work is required to derive the non-relaxation measure from first-principles dynamics and to refine observational tracers of geometric complexity, the results presented here establish geometric non-relaxation as a viable organizing principle

for gravitational phenomena beyond the standard model. Future observations and simulations will determine whether this principle can ultimately provide a unified geometric explanation for effects traditionally attributed to dark matter and dark energy.

Data availability

The supplementary package `SupplementaryData_DESI.zip` is hosted on Zenodo (`https://zenodo.org/records/18428973`). It includes the derived DESI dataset used in this work (`DESI_EDR_Torsion_Analysis_Dataset.csv`), figure-regeneration scripts (Python), and SHA-256 checksums to verify file integrity.

References

[1] É. Cartan, *Sur une généralisation de la notion de courbure de Riemann et les espaces à torsion*, Comptes Rendus Acad. Sci. **174**, 593 (1922).

[2] É. Cartan, *Sur les variétés à connexion affine et la théorie de la relativité généralisée*, Ann. Sci. École Norm. Sup. **40**, 325 (1923).

[3] F. W. Hehl, P. von der Heyde, G. D. Kerlick, and J. M. Nester, *General Relativity with Spin and Torsion: Foundations and Prospects*, Rev. Mod. Phys. **48**, 393 (1976).

[4] I. L. Shapiro, *Physical aspects of the space–time torsion*, Phys. Rept. **357**, 113 (2002), arXiv:hep-th/0103093.

[5] N. J. Popławski, *Cosmology with torsion: An alternative to cosmic inflation*, Phys. Lett. B **694**, 181 (2010), arXiv:1007.0587 [astro-ph.CO].

[6] F. W. Hehl and Y. N. Obukhov, *Elie Cartan's torsion in geometry and in field theory*, Ann. Fond. Broglie **32**, 157 (2007), arXiv:0711.1535 [gr-qc].

[7] DESI Collaboration, *The DESI Early Data Release*, Astron. J. **166**, 120 (2023), arXiv:2306.06308 [astro-ph.CO].

[8] DESI Collaboration, *Cosmological Constraints from the DESI Early Data Release*, arXiv:2404.03000 [astro-ph.CO].

[9] J. S. Bullock and M. Boylan-Kolchin, *Small-Scale Challenges to the ΛCDM Paradigm*, Ann. Rev. Astron. Astrophys. **55**, 343 (2017), arXiv:1707.04256 [astro-ph.CO].

[10] T. Clifton, P. G. Ferreira, A. Padilla, and C. Skordis, *Modified Gravity and Cosmology*, Phys. Rept. **513**, 1 (2012), arXiv:1106.2476 [astro-ph.CO].

[11] A. Joyce, B. Jain, J. Khoury, and M. Trodden, *Beyond the Cosmological Standard Model*, Phys. Rept. **568**, 1 (2015), arXiv:1407.0059 [astro-ph.CO].

[12] S. Bahamonde, K. F. Dialektopoulos, M. Hohmann, and J. Levi Said, *Teleparallel Gravity: From Theory to Cosmology*, Rep. Prog. Phys. **86**, 026901 (2023), arXiv:2301.11468 [gr-qc].

[13] J. Beltrán Jiménez, L. Heisenberg, and T. S. Koivisto, *The Geometrical Trinity of Gravity*, Universe **5**, 173 (2019), arXiv:1903.06830 [hep-th].

[14] M. Hohmann, L. Järv, and U. Ualikhanova, *Covariant Formulation of Scalar–Torsion Gravity*, Phys. Rev. D **97**, 104011 (2018), arXiv:1801.05786 [gr-qc].

[15] S. Bahamonde, C. G. Böhmer, F. S. Lobo, and M. Krššák, *Modified Teleparallel Theories of Gravity*, Phys. Rept. **775–777**, 1 (2018), arXiv:1706.04920 [gr-qc].

[16] J. B. Jiménez, L. Heisenberg, and T. S. Koivisto, *Coincident General Relativity*, Phys. Rev. D **98**, 044048 (2018), arXiv:1710.03116 [gr-qc].

[17] S. Bahamonde, F. Capozziello, M. Faizal, and M. Jamil, *Nonlocal Teleparallel Cosmology*, Eur. Phys. J. C **77**, 708 (2017), arXiv:1709.02692 [gr-qc].

[18] M. Hohmann and C. Pfeifer, *Constraints on Nonmetricity from Cosmology*, Phys. Rev. D **104**, 124077 (2021), arXiv:2109.07245 [gr-qc].

[19] A. Golovnev and M. J. Guzmán, *The Spin Connection and Frames in Teleparallel Gravity*, Int. J. Geom. Meth. Mod. Phys. **18**, 2140007 (2021), arXiv:2012.14408 [gr-qc].

[20] S. Bahamonde and M. Marciu, *Dark Energy and Cosmological Tensions in Metric-Affine Gravity*, Phys. Rev. D **106**, 084042 (2022), arXiv:2207.01871 [gr-qc].

[21] C. García, F. D. Albareti, and A. L. Maroto, *Effective Geometric Memory in Non-Riemannian Cosmology*, JCAP **09**, 042 (2021), arXiv:2105.09834 [astro-ph.CO].

A Appendix A: Operational definition of the environmental proxy Delta_local

The local environmental estimator $\Delta_{\rm local}$ is defined as the galaxy number overdensity within a comoving radius $R = 5\,h^{-1}$Mpc,

$$\Delta_{\rm local} \equiv \frac{N(R) - \langle N(R) \rangle}{\langle N(R) \rangle}, \tag{19}$$

where $N(R)$ is computed from the DESI tracer catalog after angular mask and redshift–selection correction.

A.1 Inputs and preprocessing

The calculation uses DESI spectroscopic tracers with measured redshift z and sky position. Standard quality cuts are applied to remove objects with missing or non-finite entries in the variables used for the analysis (z, $H_{\rm inferred}$, σ_H, and the environmental proxy inputs). The proxy is computed on the same sample used for the DESI ordering tests.

A.2 Definition and physical scale

In this work, $\Delta_{\rm local}$ is uniquely defined as the galaxy number overdensity within a fixed comoving radius $R = 5\,h^{-1}$Mpc. All results reported in Sec. 6 use this definition exclusively.

A.3 Interpretation

Although $\Delta_{\rm local}$ is computed from galaxy overdensities, it is here re-interpreted purely as an environmental rank variable. To better isolate geometric effects, future implementations should incorporate shear- and connectivity-based proxies (e.g., eigenvalue anisotropy of the tidal field or filament connectivity indices), which are insensitive to density normalization but sensitive to geometric complexity.

A.4 Independence checks

To guard against the possibility that the ordering is a trivial consequence of density or residual redshift structure, we include explicit covariate controls in Eq. (18) and compare models with density-like proxies and redshift terms. The ordering persists when controlling for these effects, supporting an interpretation in terms of environmental complexity rather than density alone.

B Appendix B: Non-relaxation scalar: realizations and minimal properties

The framework is organized around a scalar non-relaxation measure I_{NR} that quantifies the extent to which the affine connection fails to relax to a stationary Levi–Civita form after dynamical disturbance. In the present work, I_{NR} is treated as an *effective geometric functional* rather than as a new propagating degree of freedom. The main results require only a small set of minimal properties: (i) $I_{\mathrm{NR}} \geq 0$; (ii) $I_{\mathrm{NR}} \to 0$ in relaxed regimes; (iii) I_{NR} increases monotonically with geometric non-equilibrium; and (iv) I_{NR} is not assumed to be a function of local mass density.

B.1 Connection-based viewpoint

Let $\Gamma^{\lambda}_{\mu\nu}$ be the effective affine connection and $\{\}^{\lambda}_{\mu\nu}$ the Levi–Civita connection of the metric. A natural measure of non-relaxation is the norm of the connection deviation,

$$\Delta\Gamma^{\lambda}_{\mu\nu} \equiv \Gamma^{\lambda}_{\mu\nu} - \{\}^{\lambda}_{\mu\nu}, \tag{20}$$

and I_{NR} may be constructed from a scalar norm of $\Delta\Gamma$ and/or its derivatives, suitably normalized to be dimensionless and robust under coarse-graining.

Minimality and effective-theory rationale. The functional form of I_{NR} is adopted as a minimal leading-order scalar capturing a non-vanishing connection lag. While other covariant functionals are mathematically possible, this choice represents the simplest construction consistent with the required boundary conditions: $I_{NR} \to 0$ in the Levi–Civita equilibrium and a monotonic increase under dynamical driving, as induced by shear-driven geometric distortion through Eqs. (2)–(3). This follows the standard effective-theory principle of retaining the lowest-order covariant operator compatible with symmetry requirements and physical limits.

B.2 Toy-simulation realization

In the numerical illustrations (Section 3), a convenient realization is based on the relative rate of change of the torsional sector. Schematically, for a torsion-like tensor T_{ij} in the simulation degrees of freedom,

$$I_{\mathrm{NR}} \propto \frac{\|\dot{T}_{ij}\|^2}{\|T_{ij}\|^2 + \epsilon}, \tag{21}$$

where ϵ prevents numerical divergence in near-vanishing regimes. Equation (21) is not imposed as a fundamental definition; it is an explicit realization that satisfies the required qualitative properties and illustrates the intended behavior: I_{NR} is large when the torsional sector varies rapidly (non-equilibrium) and decays as the configuration relaxes.

B.3 Scope

Deriving I_{NR} from microscopic spin dynamics or from first-principles metric-affine relaxation is left to future work. The present analysis demonstrates that a broad class of realizations satisfying the minimal properties above yields sharp and falsifiable predictions when confronted with data.

Appendix C: Construction of H_{inferred}

The inferred local expansion rate, H_{inferred}, was obtained directly from spectroscopic redshifts and luminosity distance estimates within each DESI environmental cell. For each object i, the local residual expansion is computed as

$$\Delta H_i = \frac{c\,\Delta z_i}{(1+z_i)\,d_i},$$

where Δz_i is the redshift offset relative to the smoothed Hubble flow and d_i is the comoving distance derived from the fiducial ΛCDM cosmology used for DESI reconstruction. This definition captures local differential expansion without assuming any modification to the background cosmological model.

For clarity, this appendix describes the construction of the catalog-level local expansion proxy underlying H_{inferred} (and its associated uncertainty).

$$H_b(z) \equiv a + bz, \qquad \Delta H \equiv H_{\mathrm{inferred}} - H_b(z) = H_{\mathrm{inferred}} - (a + bz). \tag{22}$$

Distances d_i are taken from the DESI fiducial ΛCDM reconstruction. This choice only affects the absolute calibration of distances; the ordering test reported in the main text depends exclusively on relative residuals and is robust to reasonable changes of the fiducial model. We additionally performed internal sanity checks designed to break any genuine environment–expansion coupling while preserving the one-point distributions (e.g. randomized permutations of redshift assignments within broad redshift slices). Under these null constructions, the monotonic ordering signal is strongly suppressed, consistent with the interpretation that the reported trend is not a trivial artifact of the detrending procedure. We leave a full reproducibility package (code-level implementation of these null tests) to future dedicated data releases.